



Fabrication of ZIF-8/polyethersulfone (PES) mixed matrix hollow fiber membranes for O₂/N₂ separation

Alireza Hadi¹ · Javad Karimi-Sabet² · Sepehr Nikkho¹ · Abolfazl Dastbaz¹

Received: 3 November 2020 / Accepted: 5 April 2021 / Published online: 16 April 2021
© Institute of Chemistry, Slovak Academy of Sciences 2021

Abstract

This study deals with the fabrication of hollow fiber mixed matrix membrane, and evaluation its performance toward O₂/N₂ gas separation. Asymmetric mixed matrix PES membranes with embedded ZIF-8 nanoparticles as the dispersed phase were prepared by dry–wet-spinning method. The morphological, thermal, and chemical properties of spun fibers were characterized by FESEM, EDS mapping, TGA, and FTIR analysis. Effect of spinning parameters and dope composition including bore fluid/ dope flow rate ratio (0.5, 1, 2), bore fluid composition (Water/NMP: 100:0, 50:50, 75:25), polymer concentration (20%, 25%, 30%), and ZIF-8 concentration (0–40%wt at seven stages) were investigated on the morphology of hollow fiber MMMs. In addition, pure O₂ and N₂ gas permeation through the fibers was tested in order to figure out the effect of different ZIF-8 content embedded in hollow fiber MMMs on the ideal selectivity of O₂/N₂ separation. Results revealed that the maximum separation performance (ideal selectivity of 5.25) was attained at the ZIF-8 weight content of 10%. The improved performance of hollow fiber MMMs over O₂/N₂ gas separation could be related to increment in both sieving and solubility selectivity.

Keywords Mixed matrix membrane · Hollow fiber membrane · ZIF-8 · O₂/N₂ separation

Introduction

Oxygen enrichment or air separation is an inseparable part of many chemical industries. The aim of this process is to produce O₂ and N₂-enriched gaseous streams for meeting the high industrial demand. High purity N₂ is used as blanketing or purge gas in chemical industries, and for packaging purposes in food industry, while O₂-enriched gas is most applicable in combustion (Pabby et al. 2008).

There are three main methods of gas separation: cryogenic distillation, pressure swelling adsorption (PSA) and membrane separation. Membrane separation has important advantages over two other techniques such as low operating expense, modularity, and smaller units.

Polymeric membranes are favorable for gas separation applications, but the main limitation of a polymeric membrane is that it cannot provide high permeability and selectivity, at the same time. Trade-off relation between selectivity and permeability in gas separation is known as the limitation of Robeson upper bound. That is why researchers are examining different inorganic membranes such as carbon molecular sieves and zeolites for gas separation. By considering the difference between working temperatures (because inorganic membrane work at higher temperatures), these membranes have higher selectivity and permeability than polymeric membranes and their performance exceeds Robeson upper bound for the majority of gas mixtures (Nath 2008). In addition, inorganic membranes have a good mechanical strength along with high thermal and chemical stability which make them a suitable choice for separation in the harsh conditions (like high temperatures and different ranges of pH). There are important drawbacks in their applications, though. The major obstacle of inorganic membranes which limits their industrial applications is that they are much more expensive than polymeric ones (Cui and Muralidhara 2010). Another problem is scaling up, that comes from the low processability of inorganic membranes, and difficulties of placing

✉ Javad Karimi-Sabet
j_karimi@alum.sharif.edu

¹ Department of Chemical Engineering, Faculty of Engineering, University of Tehran, Tehran, Iran

² Material and Nuclear Fuel Research School (MNFRS), Nuclear Science and Technology Research Institute, Tehran, Iran

them into the large area and compact modules. In addition, inorganic membranes usually have fragile structures, and they are vulnerable against defects such as cracks which may lead to considerable negative effects on the separation process. So, the polymeric membranes are still preferred on the commercial scale. But, how to overcome the permeability/ selectivity trade-off while using polymeric membranes? As it has confirmed by many groups, the trick is to embedment of different fillers such as inorganic particles (zeolites Junaidi et al. 2014; Amooghini et al. 2016; Bastani et al. 2013) and carbonaceous materials (graphene oxide Ebrahimi et al. 2016; Li et al. 2015 and carbon nanotubes Park et al. 2016) into the polymeric phase to make mixed matrix membranes (MMMs). Indeed, MMMs combine the scalability of polymeric membranes with high selectivity and permeability of inorganic materials and offer suitable permselective properties.

The main point that should be considered in the application of MMMs is the affinity and compatibility between the polymer, filler and separation gases. Agglomeration of filler particles or particle misdistribution, particle pore blockage, chain rigidification around the filler particles, and polymer-particle interface voids or sieve-in-a-cage defect are some common problems that may occur because of thoughtless choice of MMM's components (i.e., polymer and filler) (Aroon et al. 2010). The next consideration is inherent permeability and selectivity of pure polymer material for gas pairs which is a key factor in choosing polymer matrix of MMMs (i.e., the relation between test gases and polymer matrix). Moreover, molecular diameter of separation gases should definitely be considered when filler is chosen for MMM. In other words, filler particles should make preference for desired gas molecules over undesired ones to pass from the membrane. It can be achieved by preferentially adsorption or molecular sieving properties of filler particles (i.e., filler and pair gas relation).

Recently, metal organic frameworks (MOFs) as a new type of microporous materials have gained a great importance in separation processes, especially in membrane technology. Their extraordinary properties make it possible to use MOFs themselves in the form of thin films as selective membranes for gas separation. But as discussed above, owing to their scalability, MMMs are more suitable than MOF thin films in many cases. There are numerous reports about the application of MOFs as filler in MMMs for gas separation applications (Erucar and Keskin 2011; Shahid et al. 2015; Feijani et al. 2015).

Thermal stability of MOF and its resistance to moisture are key factors which guarantee the durability of MMMs in gas separation processes. From this point of view, ZIF-8 is of the highest importance so that recently there has been great interest to use ZIF-8 as the filler in MMMs. It can be remained unchanged at up to 350 °C. In addition, ZIF-8 is

one of the most resistant MOFs against moisture. Beside its stability, with a small pore aperture of 3.4 Å, and relatively large surface area (exceeds 1800 m²/g), ZIF-8 is an appropriate candidate to be applied as dispersed phase in MMMs. Unlike flat sheet configuration, there are not many studies on the hollow fiber MMMs containing ZIF-8. Dai et al. reported asymmetric hollow fiber membranes containing ZIF-8 particles for CO₂/N₂ separation. They concluded that the addition of ZIF-8 enhances the membrane performance (Dai et al. 2012). In another work, Zhang et al. studied the effect of ZIF-8 embedding on the selectivity of 6FDA-DAM hollow fiber membranes for C₃H₆/C₃H₈ separation (Zhang et al. 2014). ZIF-8 has been successfully applied as thin film composite or mixed matrix membranes for separation of oxygen and nitrogen. Y. Liu et al. used PIM-1/ZIF-8 composite membranes for O₂/N₂ separation and their results showed enhancement in gas separation performance due to the ZIF-8 layer (Liu et al. 2019). In a very recent report, S. U. Azam et al. (2020) used ZIF-8 particles as an additive in CA membranes for O₂/N₂ separation and they observed enhancement in selectivity of this separation (Azam et al. 2020).

Owing to its high mechanical strength, good thermal and oxidative stability, Polyethersulfone (PES) is one of the most popular polymer materials in membrane applications, especially in filtration and gas separation (Zhao et al. 2013). Therefore, in this study, PES was chosen as polymer matrix for fabrication of mixed matrix hollow fiber membranes. In contrast with flat sheet membranes, hollow fiber MMMs have not been developed extensively because of their more complexity of preparation and application. In the fabrication of hollow fiber membranes, the most important issue is to control phase separation process through which desired structure would be reached. Because of multiplicity of process parameters, and sometimes their interactive effects on the final membrane morphology and performance, numerous studies have been performed on hollow fiber fabrication. Analysis of the process becomes even more complicated when molecular sieves are added to the polymer to produce mixed matrix hollow fibers.

As many factors such as membrane geometry, polymer matrix, filler type, gas pair could affect the MMMs performance in gas separation, this could be useful to present experimental data for each gas separation case. Moreover, investigation of the impact of important factors during fabrication of bare polymer and mixed matrix membranes on the morphological parameters is another goal of this study.

The first section of this study is allocated to the effect of main spinning parameters on the morphology of bare fibers. Then, mixed matrix hollow fibers with different ZIF-8 content were prepared at the ideal spinning condition obtained from the previous step. The mixed matrix fibers were subjected to gas permeation tests. Therefore, aside from the investigation of factors affecting the morphology of prepared

hollow fibers, this work is a feasibility study of O₂/N₂ separation using an innovative combination of ZIF-8 fillers and PES polymer in the hollow fiber configuration.

Experimental

Materials

Synthesis of ZIF-8 Particles

Zinc nitrate hexahydrate [Zn(NO₃)₂·6H₂O] was purchased from Sigma Aldrich. Methanol solvent, 2-methylimidazole (2-MeIM), and sodium formate (HCOONa) were purchased from Merck Co. and used as received.

Fabrication of Hollow Fibers and Gas Permeation

Polyethersulfone (PES) with molecular weight of 53,000 g/mol was purchased from BASF Corporation. N-Methyl-2-pyrrolidone (NMP) solvent was provided from Merck Co. Double distilled water was used for coagulation bath and bore fluid. Gas sources including O₂ (99.99%), and N₂ (99.99%) cylinders were supplied by Farafan Gas Co. and used for gas permeation tests without any purification.

Method

Synthesis of ZIF-8 Particles

ZIF-8 particles were prepared using room-temperature method in methanol solvent as described in our recent work (Hadi et al. 2020). Briefly, 25 ml of solutions containing zinc nitrate hexahydrate, and the mixture of 2-methylimidazole and sodium formate in methanol were prepared, separately (molar ratio of methanol: zinc nitrate hexahydrate: 2-methylimidazole: sodium formate = 1000:1:8:2). The solutions were mixed together under mild stirring for 24 h. The synthesized ZIF-8 particles separated using centrifugation (5000 rpm, 10 min). The products were repeatedly washed by acetone in order to remove remained solvent and activation of ZIF-8. The obtained solid was vacuum dried overnight to get ZIF-8 powder.

Fabrication of Bare and Mixed Matrix Hollow Fiber Membranes

Membrane dope solution was prepared by priming technique in which polymer is added to the solvent in a time programed manner. First, the weight of PES particles corresponds to each experiment in 20 ml NMP was calculated. After that, about 10% of total polymer was dissolved in NMP under mild stirring for 2 h. Then, every one hour, 30% of

polymer was added to the dope solution until the total polymer amount was dissolved. Hereafter, the prepared dope was stirred overnight, and got rest for 2 h for degassing before the spinning process. In the case of mixed matrix dope solutions, before the addition of PES, predetermined amount of ZIF-8 powder was dispersed in NMP by 1 h sonication.

Phase inversion through dry–wet-spinning technique was used to fabricate asymmetric hollow fiber membranes. Prepared dope solution and bore fluid were separately injected to the spinneret (inner/outer diameter: 0.68/1.1 mm) by two syringe pumps. After exiting from the spinneret, the nascent fibers pass the air gap distance and were precipitated by submerging in the coagulation bath. Solidified fibers are drawn by directing rolls to be collected in the take-up bath. A scheme of the spinning system has shown in Fig. 1. The spun hollow fibers were kept in distilled water for 3 days followed by 30 min in methanol in order to complete removal of water and NMP from the fiber's structure before the air-drying step. In the case of membranes used for gas separation, before air drying, coating of fibers with 3% wt polydimethylsiloxane (PDMS) solution were conducted using dip-coating method as reported elsewhere (Chen et al. 2019). Different membranes, denoted M1 to M15, were fabricated to identify the effect of dope composition and spinning condition on the morphology and properties of fibers. Tables 1, 2, 3, 4 present the fabrication condition of M1 to M15, and other fixed parameters have been reported in Tables S1 and S2.

Characterization

Filler particles and MMMs were characterized for investigating their morphology and features. FESEM images of ZIF-8 particles were taken by a TESCAN MIRA3 field emission scanning electron microscope. Small amount of ZIF-8 synthesis solution was dropped on the substrate and dried at ambient temperature. XRD spectrum of ZIF-8 particles was obtained using a X'Pert PRO MPD diffractometer (PANalytical Company) using Cu K α radiation ($\lambda = 1.5406 \text{ \AA}$) that was operated at 40 kV and 40 mA. Scanning electron microscopy (SEM) of cross section, inner and outer surface of prepared hollow fiber membranes were captured using a TESCAN VEGA3 scanning electron microscope. A TESCAN MIRA3 microscope was also used for capturing high magnification FESEM images and EDS mapping analysis of hollow fiber cross sections. In order to analysis cross section of membranes, fibers were fractured in liquid nitrogen. SEM Samples for observation of the inner surface of fibers were prepared by fixing the membranes on a piece of tape, cutting fibers through their length direction, and spreading them on the tape. Morphological parameters of fibers including inner and outer diameters, wall thickness, and porosity were calculated by analysis of cross-section SEM images using ImageJ software 1.46r (NIH, USA). It worth

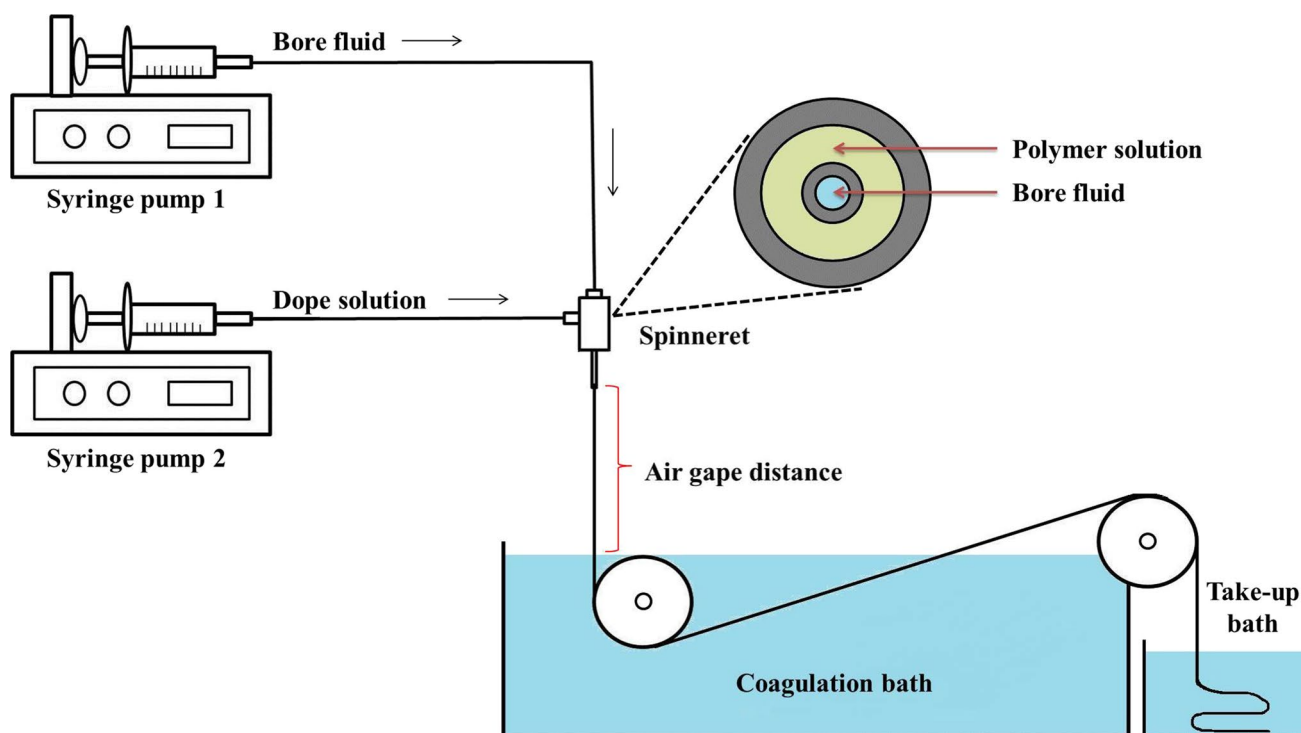


Fig. 1 Schematic representation of hollow fiber dry-wet-spinning apparatus

Table 1 Dope composition and membranes ID for investigation of polymer concentration's effect

Parameter	Membrane ID	Dope composition/wt%			
		Polymer (PES)	Solvent (NMP)	VS (THF)	NSA (Ethanol)
Polymer concentration	M1	20	60	5	15
	M2	25	55	5	15
	M3	30	50	5	15

Table 2 Experimental condition and membranes ID for investigation of internal coagulant's effect

Parameter	Membrane ID	Composition/wt%	
		Internal coagulant	
		Water	NMP
Internal coagulant	M4	100	0
	M5	75	25
	M6	50	50

mentioning that the porosity of membranes was defined as the ratio of macro-voids surface area to the total membrane cross-section area. Thermogravimetric analysis was conducted

Table 3 Experimental condition and membranes ID for checking the effect of dope and bore fluid flow rates

Parameter	Membrane ID	Flow rates/ml/min	
		Dope	Bore
Dope solution and bore fluid flow rates	M7	2	1
	M8	1	1
	M9	1	2

using a Rheometric scientific STA 1500, with the heating rate of 10 °C/min.

Permeability and Selectivity Measurements

Permeation measurements of spun hollow fibers were conducted by experimental gas permeation setup which is schematically shown in Fig. 2. This gas permeation system was designed to operate on constant volume—variable pressure mode.

Permeability as an important factor toward evaluation of the membrane performance was defined according to Eq. 1.

$$P = \frac{273.15 \times 10^{10} \times V \times l}{760 \times A \times T \times \Delta P_0} \times \frac{dP}{dt} \quad (1)$$

Table 4 Dope composition and membranes ID for MMMs with different ZIF-8 content

Parameter	Membrane ID	Dope composition/wt%				
		Polymer (PES)	Solvent (NMP)	VS (THF)	NSA (Ethanol)	ZIF-8/PES (wt%)
ZIF-8 concentration	M10	20	60	5	15	0
	M11	20	60	5	15	5
	M12	20	60	5	15	10
	M13	20	60	5	15	20
	M14	20	60	5	15	30
	M15	20	60	5	15	40

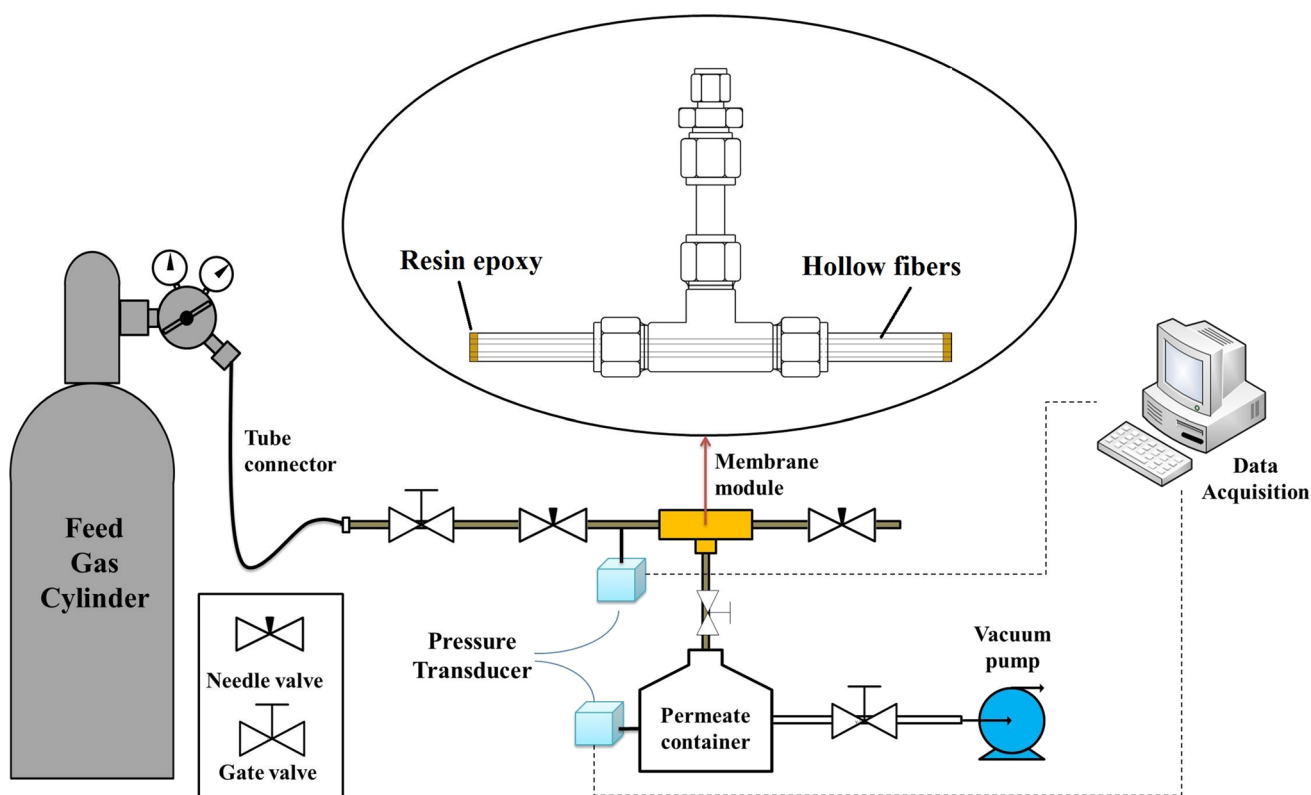


Fig. 2 Schematic illustration of gas permeation system

In this equation, P is permeability [$\text{cm}^3(\text{STP})\cdot\text{cm}/\text{cm}^2\cdot\text{cmHg}\cdot\text{s}$], V stands for the volume of permeate chamber (cm^3), l is the skin layer thickness, A is the effective surface area of membrane (cm^2), T is temperature (K), ΔP_0 denotes the trans-membrane pressure (cmHg), and (dP/dt) refers to pressure gradient of permeate side (cmHg/s). Permeation tests were conducted using a homemade stainless-steel module containing two fibers (shown in Fig. S1). The open ends of fibers were potted in epoxy resin, and the effective surface area of each membrane was around 2.25 cm^2 . Before the permeation tests, the apparatus was evacuated for 4 h until it reaches to 0.05 mbar. Permeation tests were carried out by applying

trans-membrane pressure of 2 bar at the temperature of $35 \text{ }^\circ\text{C}$. Equation 2 is used to obtain the ideal selectivity of gas pairs which is defined by dividing permeability values of two gas.

$$\alpha_{ij} = \frac{P_i}{P_j} \tag{2}$$

Results and Discussion

Characterization of ZIF-8 Particles

The morphology of prepared ZIF-8 particles as the additive of membranes was investigated using FESEM images. Figure 3 shows the FESEM image of synthesized ZIF-8 particles alongside with the corresponding particle size distribution. ZIF-8 particles with rhombic octahedron morphology and well-defined edges could be observed in this figure. Particle size analysis showed that ZIF-8 powder with mean particle size of about 240 nm was obtained at our synthesis condition.

Figure 4 presents the X-ray diffraction pattern of prepared ZIF-8 material along with the indexing of different crystalline planes. Main characteristic ZIF-8 peaks could be observed in XRD pattern of the prepared sample containing diffraction peaks located at 2θ angles of about 7.35° , 10.4° , 12.75° , 14.73° , 16.48° , and 18.07° which are labeled as (011), (002), (112), (022), (013) and (222) crystal facets in Fig. 4. The presence of all main ZIF-8 diffraction peaks with high intensity verifies the high quality and crystallinity of the products.

In order to probe the chemical structure of ZIF-8 particles, FTIR spectra could be useful which shown in Fig. S2. In this figure, peaks arise at about 690 and 760 cm^{-1} are attributed to aromatic C-H bending, while peaks at $900\text{--}1400\text{ cm}^{-1}$ are related to C-N bonds. The band at 1580 cm^{-1} associated with C=N stretching, and peak at

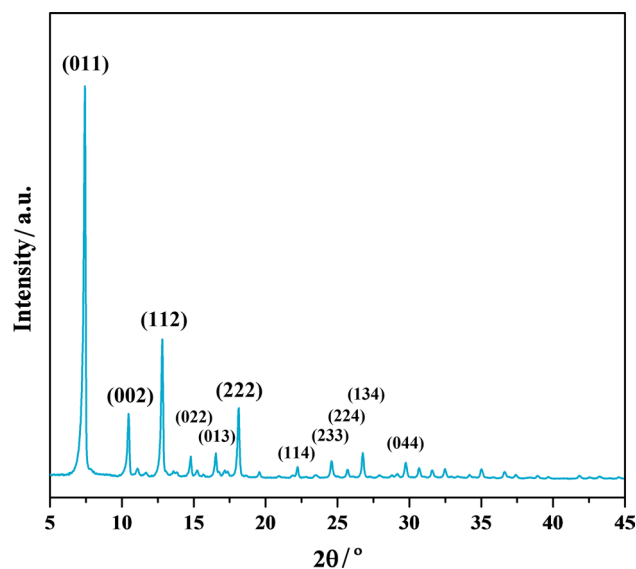


Fig. 4 XRD pattern of synthesized ZIF-8 nanoparticles

2928 cm^{-1} is due to the aromatic stretching of C-H. The peak at about 3128 cm^{-1} corresponds to aliphatic C-H stretching modes of the imidazole in ZIF-8.

In addition, N_2 adsorption–desorption isotherm is one of the important characterization techniques for porous materials. Our recent work (Hadi et al. 2020) showed that ZIF-8 microporous particles with surface area higher than $1200\text{ m}^2/\text{gr}$ could be synthesized by room temperature method which seems ideal for gas separation applications.

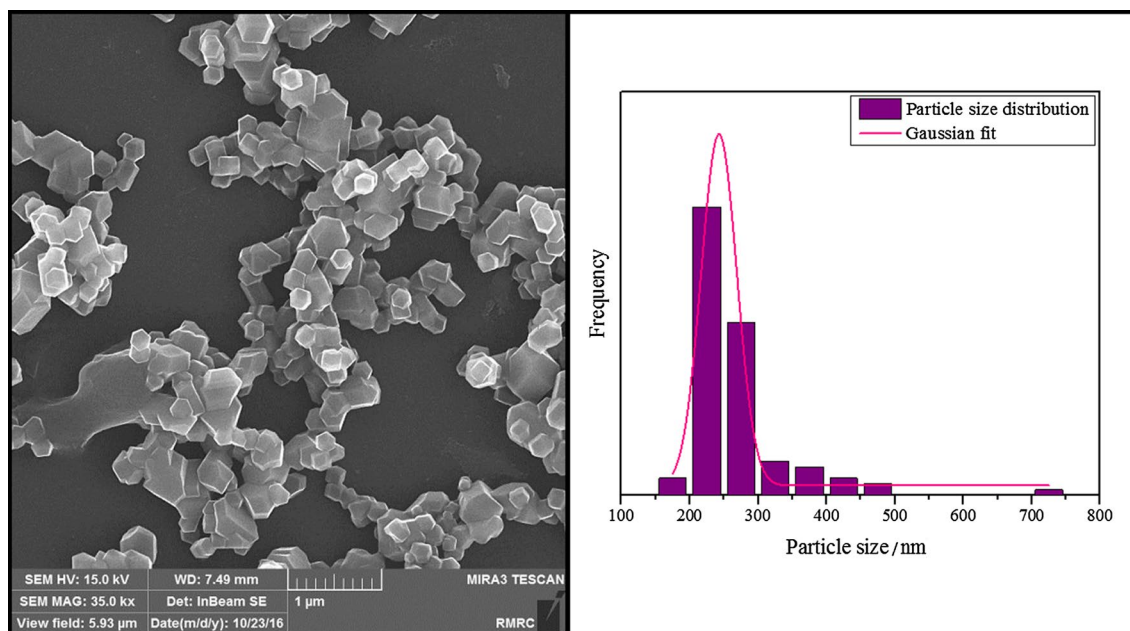


Fig. 3 FESEM image of prepared ZIF-8 sample (left), and particle size distribution of ZIF-8 particles (right)

Characterization of Hollow Fiber Membranes

Effect of Fabrication Parameters on the Morphology of Membranes (SEM Analysis)

SEM images were utilized to probe the impact of chosen factors including dope composition (polymer concentration and filler content) and spinning condition (bore fluid composition and extrusion flow rates) on the hollow fiber's morphology and physical properties.

Generally, asymmetric hollow fiber membranes are known to have the structure consists of a porous support underneath the selective skin layer. It has been proved that high phase separation rates result in finger-like macro-voids, while sponge-like structure would be formed if delayed

phase separation is provided by some techniques. In this study, THF and ethanol were used in the dope solution as volatile solvent for preparing a non-defective skin layer, and non-solvent additive for controlling macro-void formation, respectively.

It is well understood that the morphology and particularly the pore structure of polymeric membranes are controlled by the phase separation mechanism. Both thermodynamic and kinetic effects contribute to the phase separation process. The SEM images which have been presented in this section (Figs. 5, 6, 7) showed that the predominant morphology of spun fibers is cellular (closed cell pore structure). Therefore, it can be inferred that the phase separation mechanism is nucleation and growth with relatively fast solidification process (Nunes and Peinemann 2006).

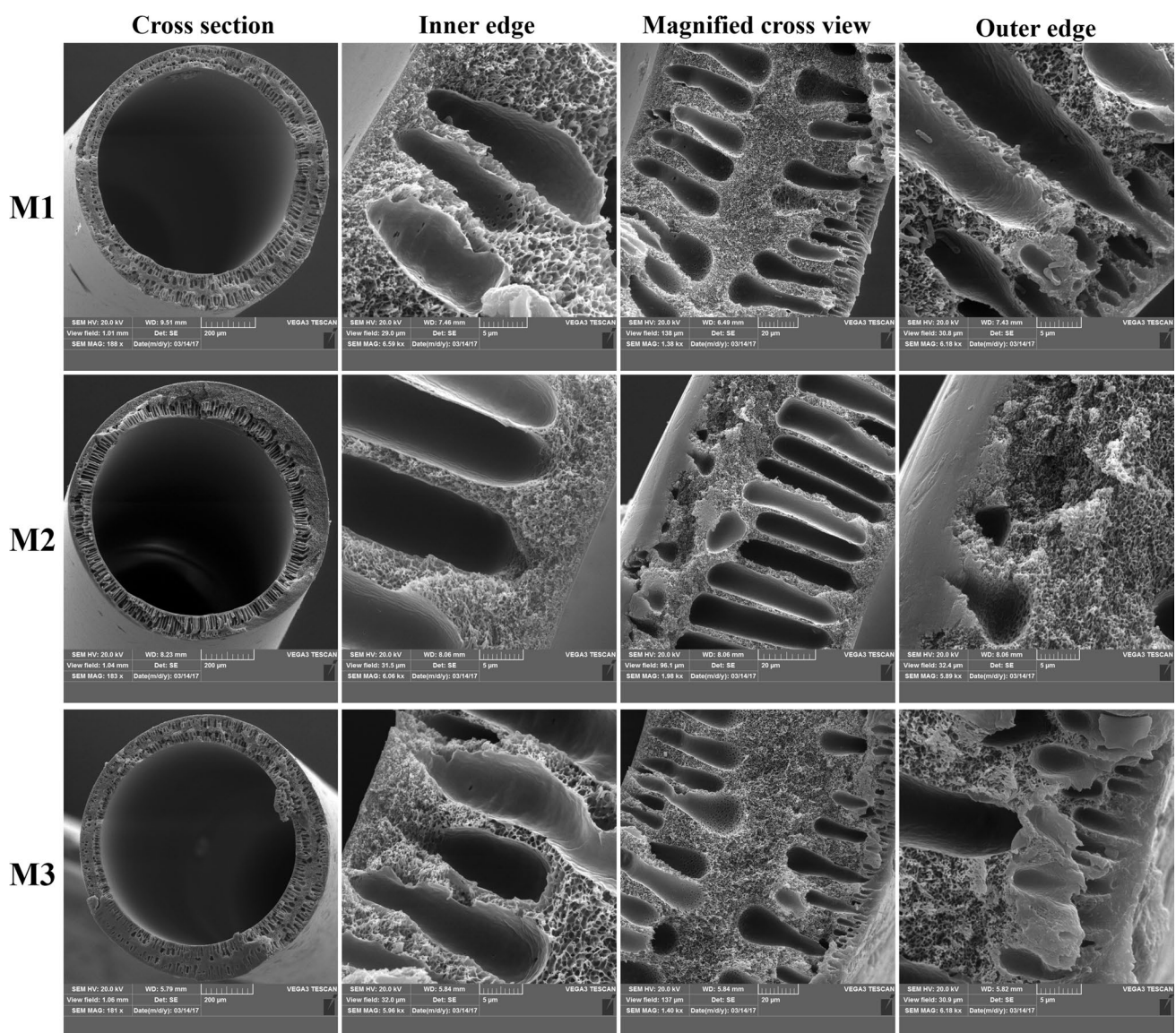


Fig. 5 SEM micrographs of cross-section views of hollow fibers prepared from different polymer concentration from 20 to 30% (M1–M3)

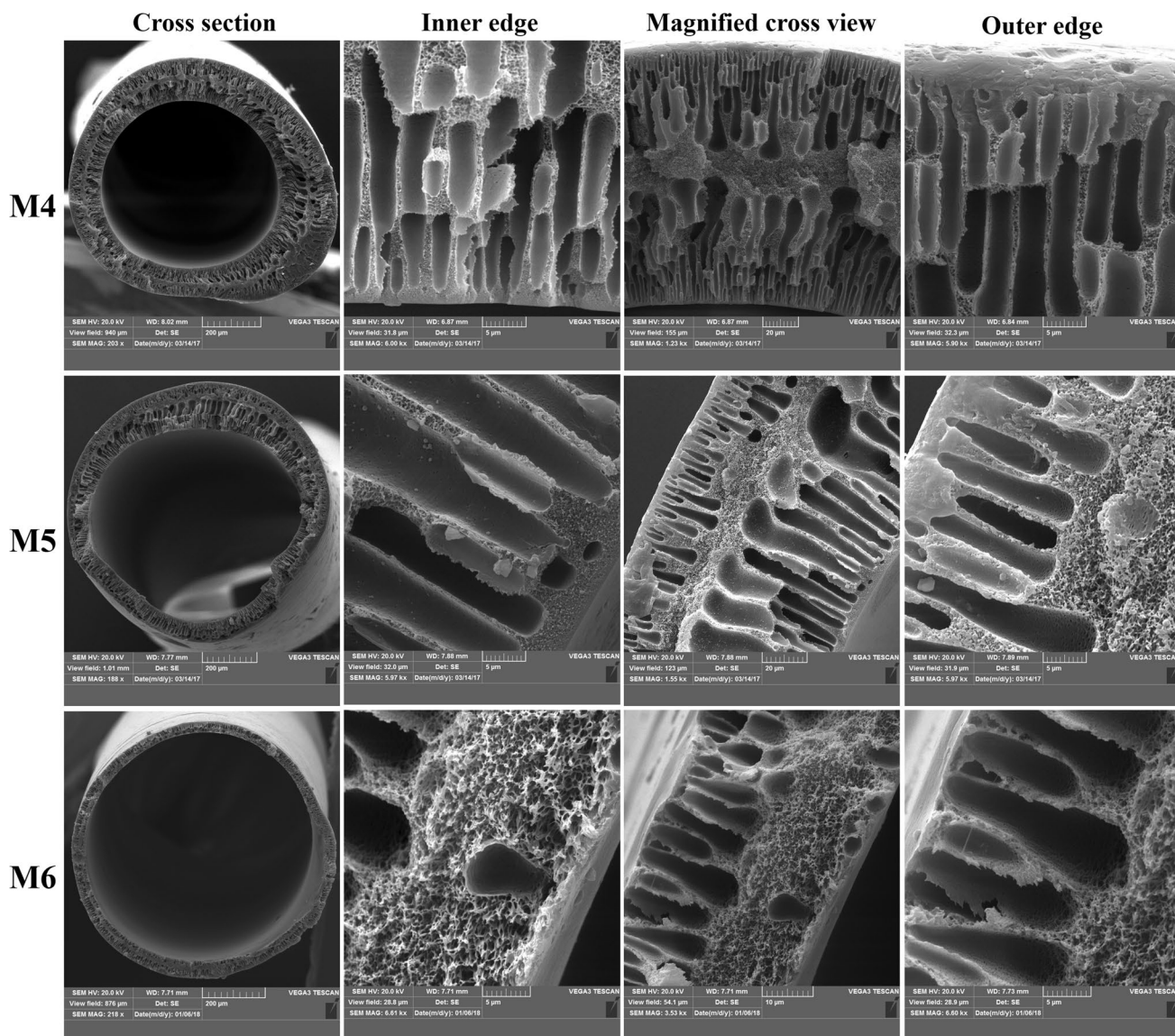


Fig. 6 SEM micrographs of cross-section views of hollow fibers prepared with different internal coagulant composition containing 0–50% of NMP (M4–M6)

The first parameter is polymer concentration of the dope solution. Figure 5 shows the SEM images of hollow fibers synthesized from different PES concentration. In addition, the quantitative results and morphological features of hollow fibers (fabricated at different spinning conditions: M1–M9) obtained from SEM analysis have been presented in Fig. S3 to S5. Dope solution viscosity is the main feature that affected by changing the polymer concentration. As it was expected, increasing the polymer concentration resulted in thicker skin layer and lower porosity (reduction of the number and size of macro-voids) of the membranes. Indeed, increase in polymer concentration and higher dope viscosity leads to restricted solvent and non-solvent exchange or delayed demixing during the precipitation process. By

increasing the PES concentration to 25% (M2), the outer edge finger-like macro-voids have been disappeared. At the polymer concentration of 30% (M3), the outer edge macro-voids appeared again and M3 has smaller inner and outer edge macro-voids.

According to the results, a steep incline of about 200 μm occurs in fiber thickness when the PES concentration rises from 20 (M1) to 25% (M2) which comes from the higher viscosity of M2 that limits the gravity effect. But further increase in the polymer concentration to 30% (M3) results in the slight decline in fiber thickness but still thicker than that of 20% (M1). As could be seen from Fig S2, both inner and outer fiber diameters have a rising trend with polymer concentration in the range of 20–30%. The reduction of

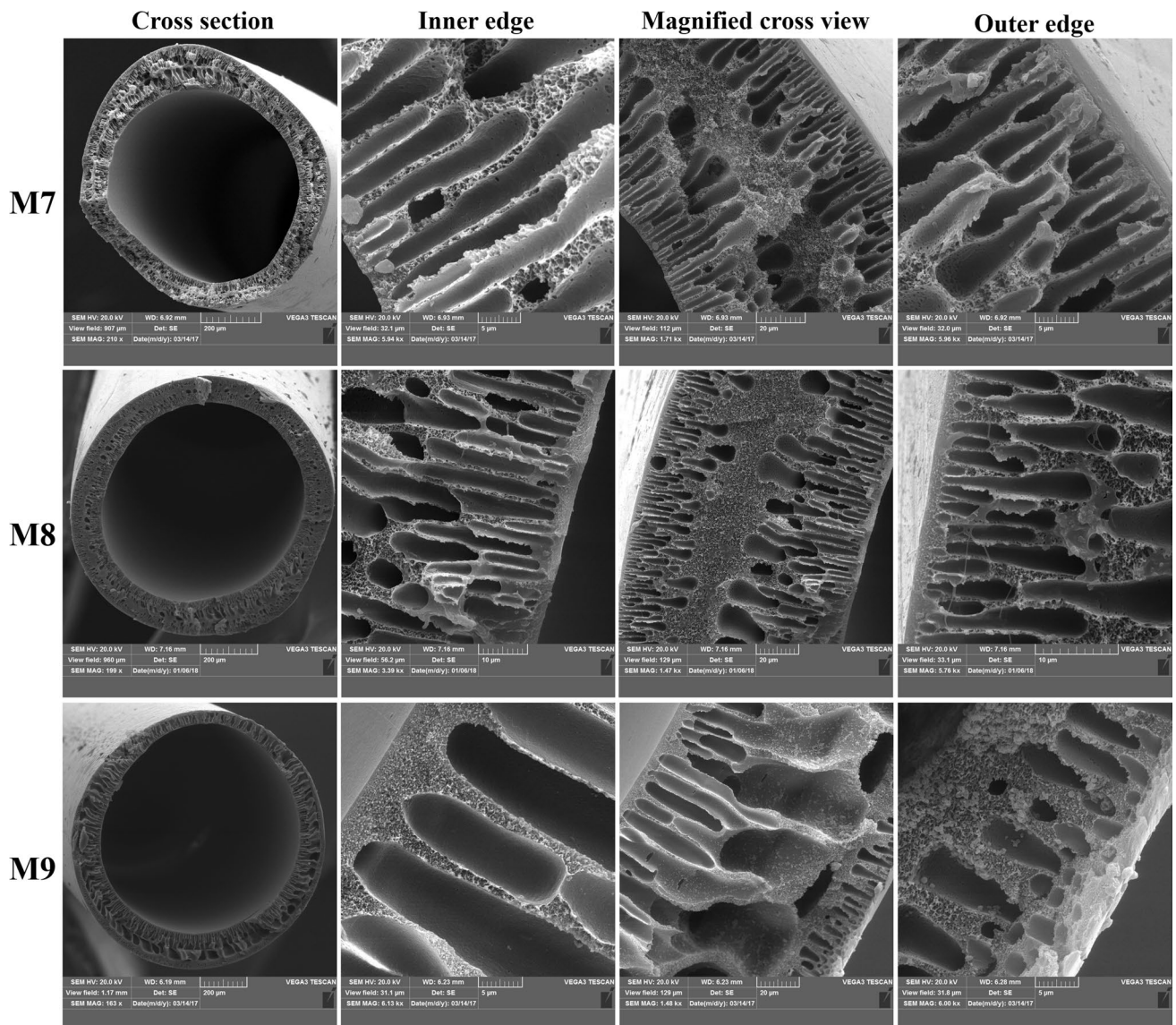


Fig. 7 SEM micrographs of cross-section views of hollow fibers fabricated by different dope/bore fluid flow rate ratios from 2 to 0.5 (M7–M9)

thickness from M2 to M3 could be related to the residence time of nascent fibers in the air gap distance. It has been proved that the fiber thickness is influenced in the air gap distance through the gravity effect on nascent fibers. Increasing the PES concentration to 30% results in the significant viscosity rise which extends the residence time of nascent fiber in the air gap. Therefore, higher elongation effect in the air gap suppresses the rising trend of outer diameter in comparison to the inner diameter, and the thickness reduces, consequently.

Figure 6 represents the impact of bore fluid composition on the morphology of hollow fibers. This parameter could alter the structure of inner skin and the inner layer of porous support. By increment of the NMP content from 0 to 50% (M4–M5 samples), the thickness of inner skin layer

significantly rises, but the inner finger-like voids become larger. While rising the NMP content from 25 (M5) to 50% (M6) leads to disappearing of inner macro-voids and thinner skin layer. Adding a small amount of NMP solvent to the bore fluid brings the system to a more stable condition which decreases the rate of phase inversion and results in the denser inner skin. This effect becomes more pronounced when the NMP content further increases to 50% for M6 which leads to disappearing of inner edge macro-voids and lower porosity of M6 sample.

According to Fig S4, increasing in the NMP content from 0 (M4) to 25% (M5) in the bore fluid made both inner and outer diameter rise. By further increment in the NMP content to 50% (M6), a slight increase in the inner diameter accompanied by decrement in the outer diameter which

resulted in the steep decline in the fiber thickness. Similar results were obtained for thickness change with internal coagulant composition in Simone et al. work (Simone et al. 2014). By addition of solvent to bore fluid, the phase inversion rate and in turn the solidification rate of nascent fibers in the air gap reduces. Therefore, the nascent fibers are more affected by the gravity and the resultant fibers become thinner. In addition, the increasing of inner diameter at higher NMP content could be explained by the higher effect of shear forces originate from bore fluid flow on the unsolidified nascent fibers in the air gap distance.

Cross-section SEM images of fibers obtained from various dope/bore fluid flow rate ratios have been shown in Fig. 7. This factor had the most effect on the porosity of prepared fibers among the studied parameters (Fig. S7). This figure suggests that the thickness, inner and outer diameters increase with dope/bore flow rate ratio. When the bore fluid flow rate increases, the higher pressure of bore fluid makes the inner diameter larger. The outer diameter increment from dope/bore flowrate ratio of 2 (M8) to 0.5 (M9) could be due to the effect of higher bore flowrate on the unsolidified nascent fibers.

The porosity value of spun fibers of M7, M8, and M9 (with dope/bore flowrate ratios of 2, 1, and 0.5, respectively) has been shown on Fig. S5. The M8 had the lowest porosity which could be related to the lower phase separation rate because of the lower bore and dope flow rates. According to the above explanations the dope/ bore flowrate ratio of 1:1 was chosen for preparation of MMMs (M10–M15) investigating the effect of filler content.

The effect of ZIF-8 content on the morphology of MMMs could be explained by viscosity change of dope solution. Increasing the filler content results in the higher viscosity of dope solution which in turn declines the porosity of MMMs. This trend could be observed by increasing the ZIF-8 content from 0 (M10) to 10% (M12), but incorporating the higher amount of ZIF-8 leads to higher porosity (Fig. 8). As could be seen from Fig. S6, by increasing the filler content from 0 (M10) to 10% (M12), the dense region between inner and outer finger-like macro-voids becomes larger, but by further increment in ZIF-8 content (10–40%), this region becomes smaller. This is due to very slow phase separation at high ZIF-8 concentrations leading to a thick and dense skin layer at outer edge of the fibers, which results in the restricted

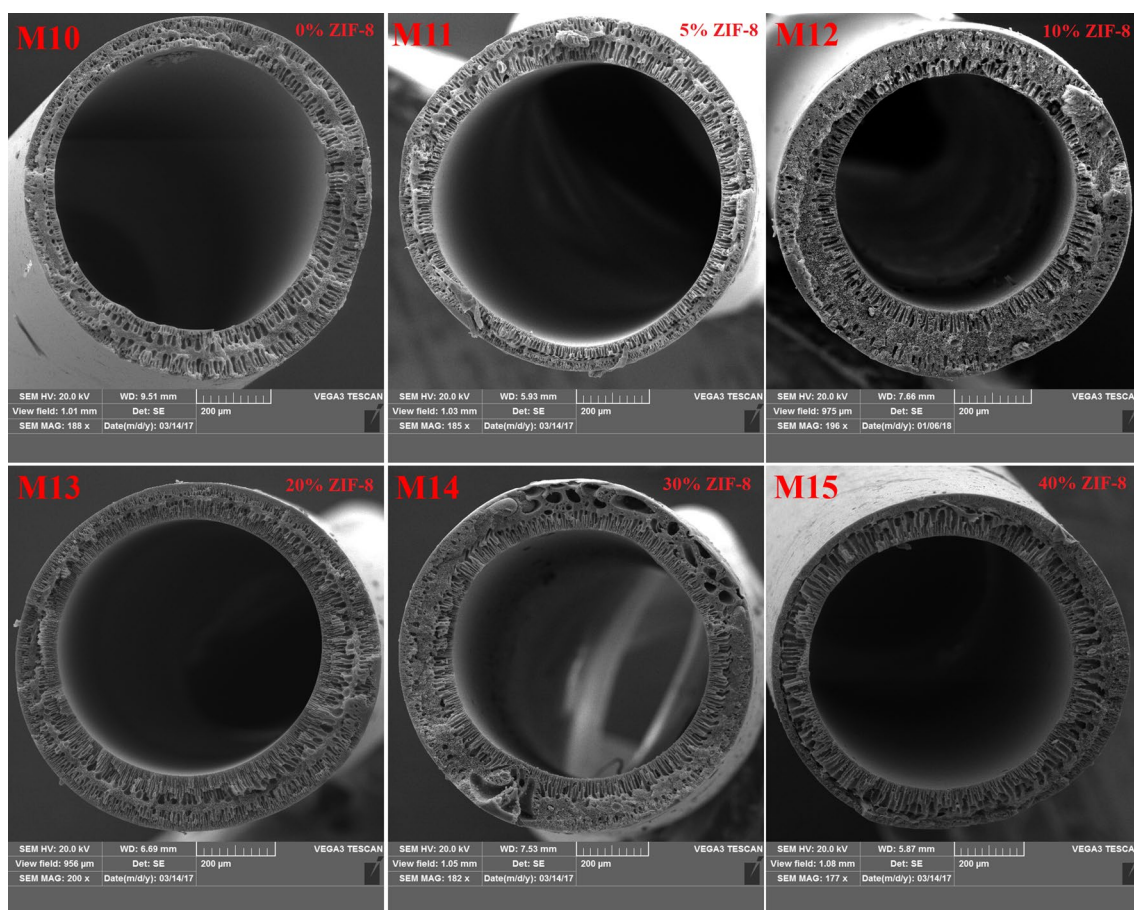


Fig. 8 Cross-section SEM micrographs of hollow fibers containing 0–40% ZIF-8 particles (M10–M15)

solvent and non-solvent exchange process during phase inversion in the coagulant bath. This phenomenon is pronounced for the highest ZIF-8 concentration of 40%, results in disappearing of outer edge fingers and a gap between the outer and inner layers of fibers which could be seen from cross-section view of M15 sample (Fig. S6).

Effect of filler content on the thickness of the prepared fibers has been illustrated in Fig. 9a. For ZIF-8 content of 0% (M10) and 5% (M11), the fiber thicknesses are about 100 and 110 μm . The M12 (10% ZIF-8) sample with the mean wall thickness close 150 μm had the maximum value. The wall thickness of M13 (20% ZIF-8) to M15 (40% ZIF-8) fluctuates between about 120 to 140 μm . As shown in Fig. 9b, M12 with 10% of filler content had the lowest porosity among the MMMs. In spite of the fact that M15 had the highest viscosity, it had the highest porosity, too. This is due to the defective void in the M15 structure which formed as a gap inside the fiber.

High magnification FESEM analysis was employed in order to have an insight into the effect of ZIF-8 embedment on the polymer morphology in the support layer and the skin layer thickness. Fig. S7 illustrates the high magnification FESEM of the cross sections of MMMs with different amount of ZIF-8. The cross sections were taken from the porous support layer. As could be seen from the figure, the bare PES membrane has a nearly nodular structure. By increasing the filler content, the continuity of the polymer matrix increases, and the matrix structure becomes cellular-like, so that larger voids are formed in the support layer where the filler particles agglomerate in. This seems to affect the mechanical strength of the hollow fiber MMMs. The change in the morphology of polymer matrix could be related to the viscosity change of the dope solution and different demixing rates during phase inversion.

For explore the distribution of filler particles in the hollow fiber MMM, EDS mapping of Zn element (as the main indicator of ZIF-8 material) has been taken from one of the samples which shown in Fig. S8. The figure indicates the well distribution of ZIF-8 particles in the porous support layer.

In addition to the ZIF-8/polymer in the support layer of hollow fibers, we checked the level of ZIF-8/PES interaction in the skin layer which is a more prominent factor in the gas separation performance. This was conducted by high magnification FESEM image of the surface of inner skin layer of the M12 (containing 10% MOF) which is shown in Fig. S9. As illustrated in this figure, ZIF-8 particles are completely surrounded by dense polymer skin layer and the adhesion of the fillers to matrix is suitable which shows the satisfying affinity of filler particles and PES matrix.

The skin layer of hollow fiber has a crucial role in gas separation applications. In most cases, the precise determination of the skin layer thickness is difficult. High magnification FESEM images of MMMs cross section have been shown in Fig. S10 to roughly determine the impact of filler content on the skin layer thickness. As can be observed, by addition of ZIF-8 filler, the outer skin layer of fibers becomes thicker which may contribute to the better gas separation performance of MMMs in comparison with bare PES. Although the skin layer thickness of M12 (10% ZIF-8) sample could not be determined precisely, but its skin layer is denser than other samples.

Besides from the cross-section views of the membranes, the SEM micrographs of the inner and outer surface of spun fibers give information about the morphology of MMMs. The SEM images of inner and outer surface of M10–M15 samples are presented in Fig. 10 and Fig. S11, respectively. As could be seen in these figures, the morphology of the

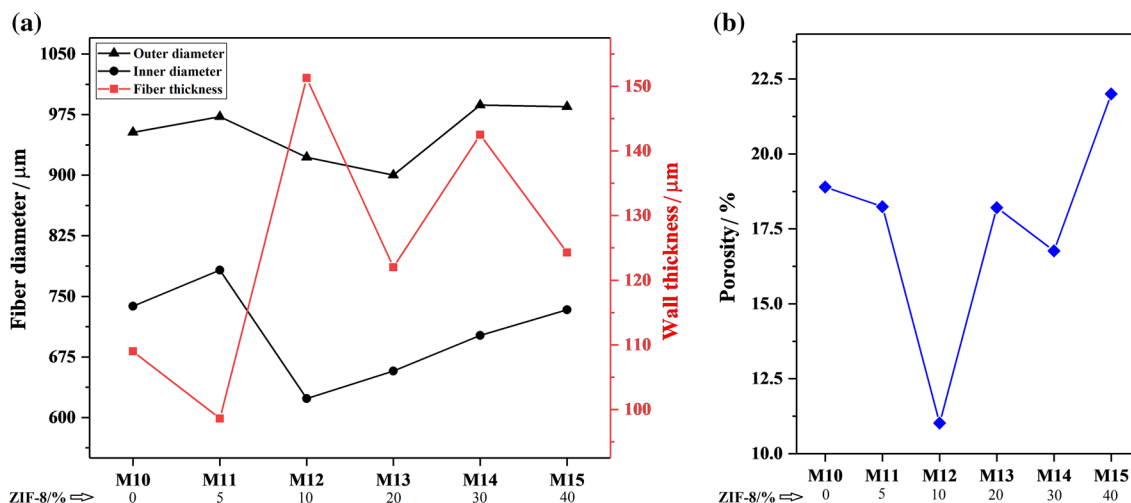


Fig. 9 Effect of ZIF-8 content from 0 to 40% (M10–M15) on the morphological characteristics of hollow fiber MMMs

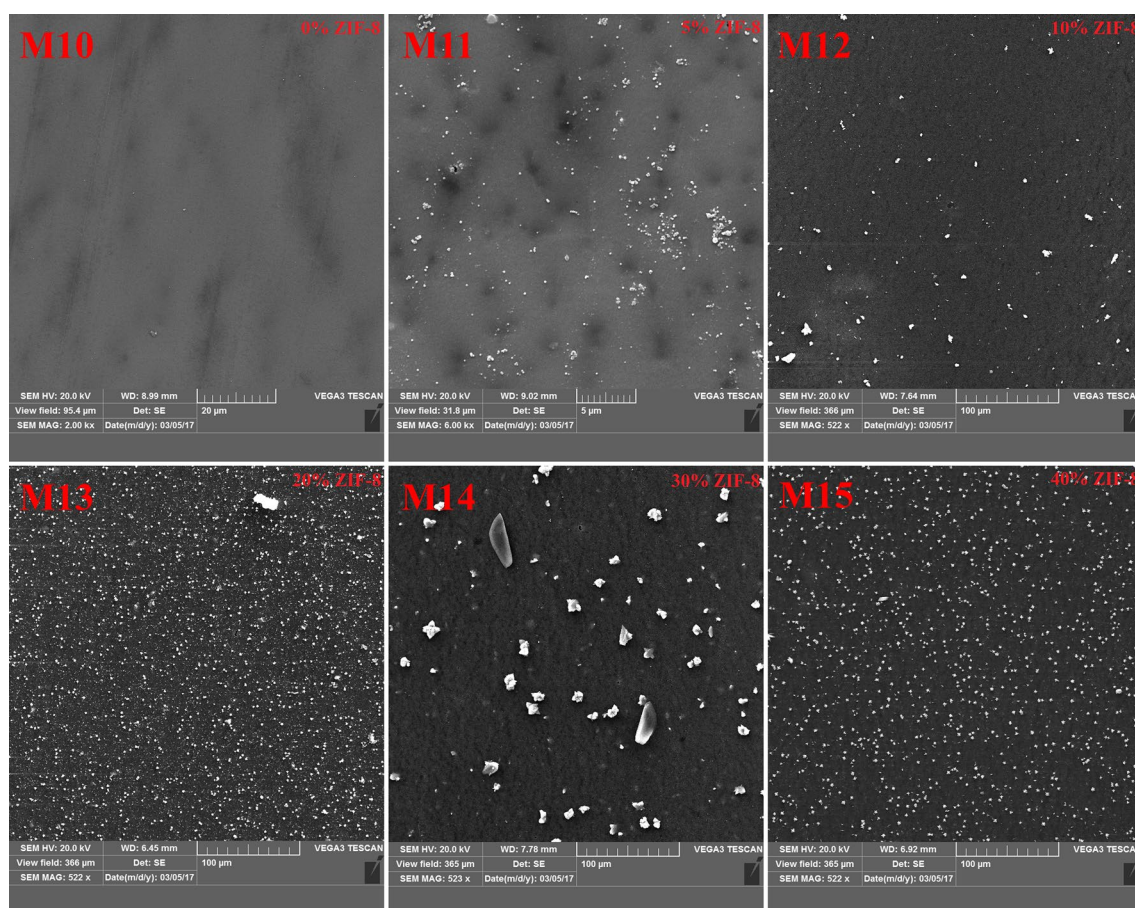


Fig. 10 SEM images of the inner surface of hollow fiber MMMs (M10–M15)

outer surface of the fibers is featureless and does not contain ZIF-8 particles. On the contrary, the ZIF-8 particles could be seen clearly in the SEM micrographs of the inner side of the MMMs, and in most cases the density of particles on the inner surface increases with the ZIF-8 content from M10 to M15.

Based on the SEM images of hollow fibers, Fig. 11 could be inferred as the scheme of MMMs morphology and separation mechanism.

FTIR Spectra of Hollow Fibers

Surface chemistry of hollow fibers was characterized by FTIR analysis. Figure 12 shows the FTIR spectra of hollow fiber membranes containing different amount of ZIF-8 particles ranging from 0 to 40%wt (M10–M15). Various chemical groups present in the membrane structure could be recognized through investigation of identifying peaks in the infrared spectroscopy. According to the chemical structure of PES which contains a benzene ring, sulfone and ether groups, different peaks could be assigned. Strong peaks located at 1485 and 1577 cm^{-1} are related to benzene ring.

The absorption bands at 1105, 1149, 1298 and 1323 cm^{-1} are attributed to symmetrical and asymmetrical stretches of (O=S=O) group. In addition, strong peak appeared at around 1240 cm^{-1} was assigned to stretching vibration of (C–O–C) bond (Han et al. 2010; Hasanajili et al. 2017). As could be seen from this figure, different synthesized membranes have very similar spectra. It means that ZIF-8 particles could not be detected in the FTIR spectra. This observation further confirms the low amount of ZIF-8 particles on the surface of fibers. However, by increasing the ZIF-8 content in the samples, some weak peaks emerge in the wavenumbers between 2250 and 2500 cm^{-1} , and the intensity of these peaks becomes slightly higher by ZIF-8 content which could be a sign of low ZIF-8 amount on the surface of MMMs.

TGA and DSC Analysis of Membranes

Figure 13 illustrates the TGA curves of ZIF-8, PES, and MMMs with different filler content. Different samples experienced two (as-synthesized ZIF-8, and unfilled PES) or three weight loss steps (MMMs) during heating at temperatures in the range of 20–800 °C. The

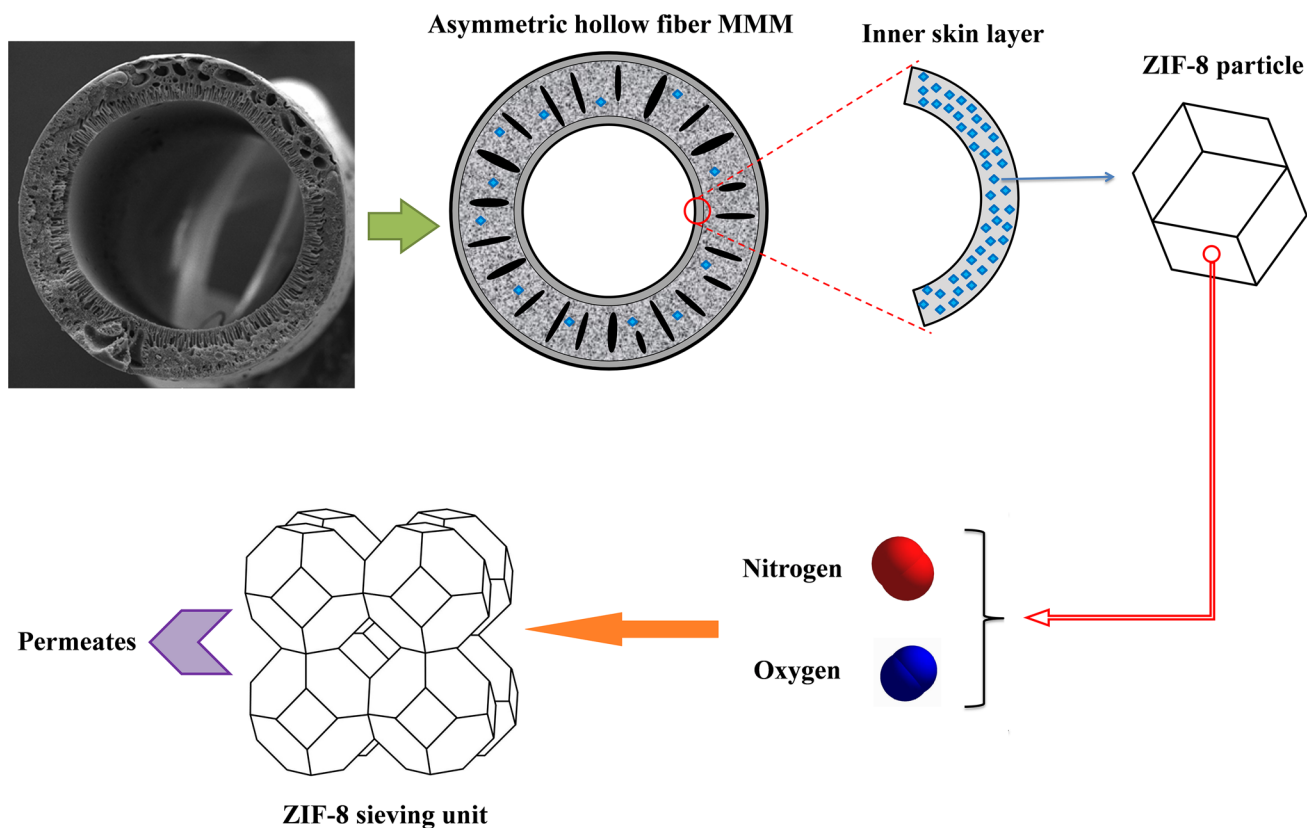
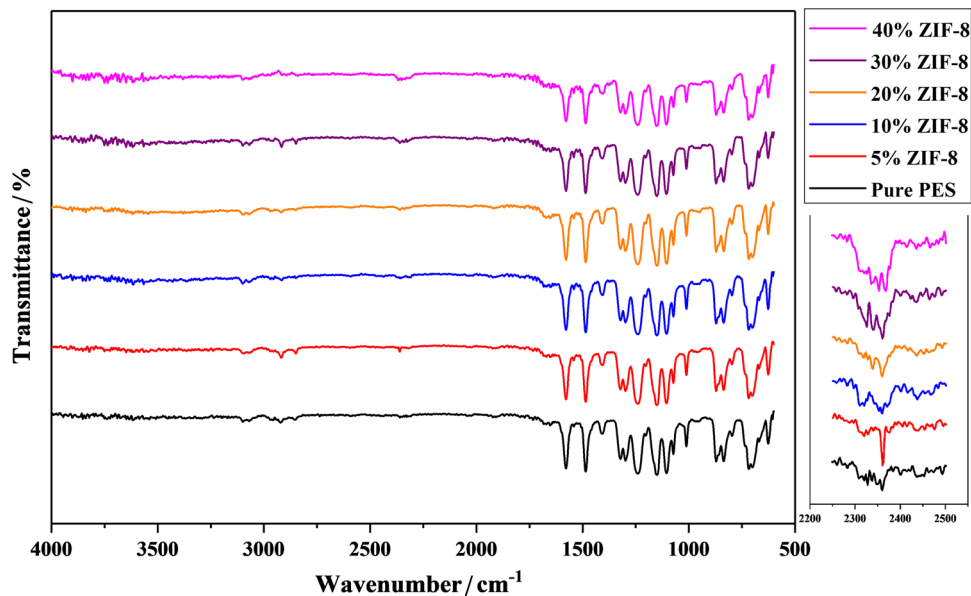


Fig. 11 Schematic drawing of the morphology of fabricated hollow fibers and molecular sieving effect

Fig. 12 FTIR spectra of hollow fiber MMMs with different amount of ZIF-8 particles



first weight reduction (less than 10%) at about 200 °C is related to NMP solvent evaporation from the membranes which could be seen for all samples with 0–40% ZIF-8 (M10–M15). According to TGA thermograms, the decomposition temperature of PES is about 500 °C, and

embedding of MOF has slightly declined the thermal stability of composite. Considering Fig. 13, the degradation temperature (T_d) of ZIF-8 particles is about 130 °C lower than that of pure PES polymer. Except M11 (ZIF-8 loading of 5%) which has a completely the same TGA curve

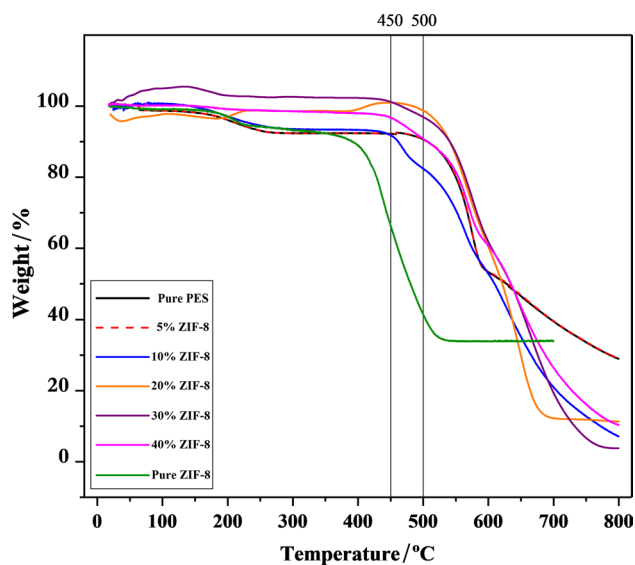
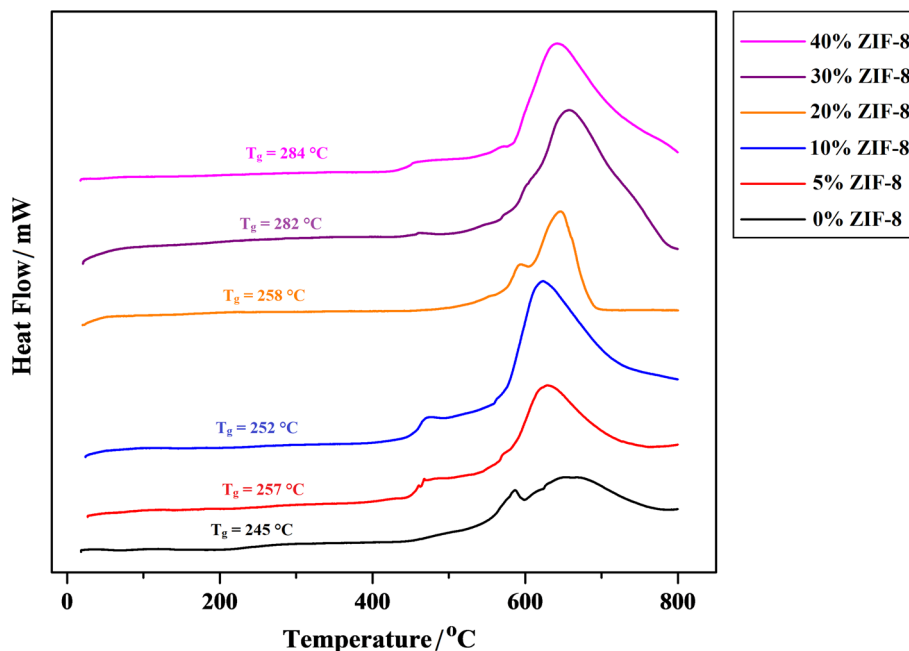


Fig. 13 TGA curves of ZIF-8 particles, PES (M10), and MMMs (M11–M15)

as unfilled PES, T_d of other MMMs did not change more than 50 °C relative to pure PES, and this reduced thermal stability of MMMs is due to the mixing of polymer matrix with lower thermally stable MOF material. Indeed, for the MMMs, there is a second weight loss step (at ~450 °C) of about 10% before the main stage (at ~500 °C) which could be related to degradation of organic ligand functional groups in ZIF-8 and/or removal of trapped solvent molecules in the ZIF-8 pores. In the case of MMMs the third stage occurs at 500 °C which is ascribed to PES decomposition.

Fig. 14 DSC curves of PES (M10), and MMMs (containing 5–40% ZIF-8)



Differential scanning calorimetry is a common technique for evaluation of compatibility between filler and polymer matrix in MMMs. This investigation is performed by the change in glass transition temperature of composite membranes. Figure 14 shows DSC traces of hollow fiber MMMs (M10–M15) undergoing a temperature rise from 20 to 800 °C. According to this figure, by increasing the ZIF-8 content in the PES matrix, the glass transition temperature (T_g) and melting temperature (T_m) have changed. For all samples, DSC curves showed an endothermic peak centered at melting temperature of composite. The melting temperature of all MMMs shifted to lower values relative to that of unfilled PES (at around 650 °C). As shown in Fig. 14, T_g increased from 245 to 282 °C for M10 (0% ZIF-8) to M15 (40% ZIF-8), respectively. M11 (5% ZIF-8) sample is an exception for the ascending trend of T_g with ZIF-8 content that could be caused by the experimental error. Indeed, the embedding of ZIF-8 particles to a certain extent leads to weaker polymer chain mobility due to the chain rigidification around the MOF particles as the nucleus for polymer crystallization which raises the T_g , consequently. Therefore, increase in T_g by introducing the ZIF-8 materials into PES resulted from the limited chain flexibility and formation of intermediate trans-crystalline phase at polymer matrix-filler interface. This observation approves the high affinity between PES matrix and the ZIF-8 particles.

Permeability and Selectivity of MMMs

Gas separation performance of the bare PES and mixed matrix hollow fibers for O₂/N₂ gas pair was evaluated using constant volume- variable pressure method. Figure 15

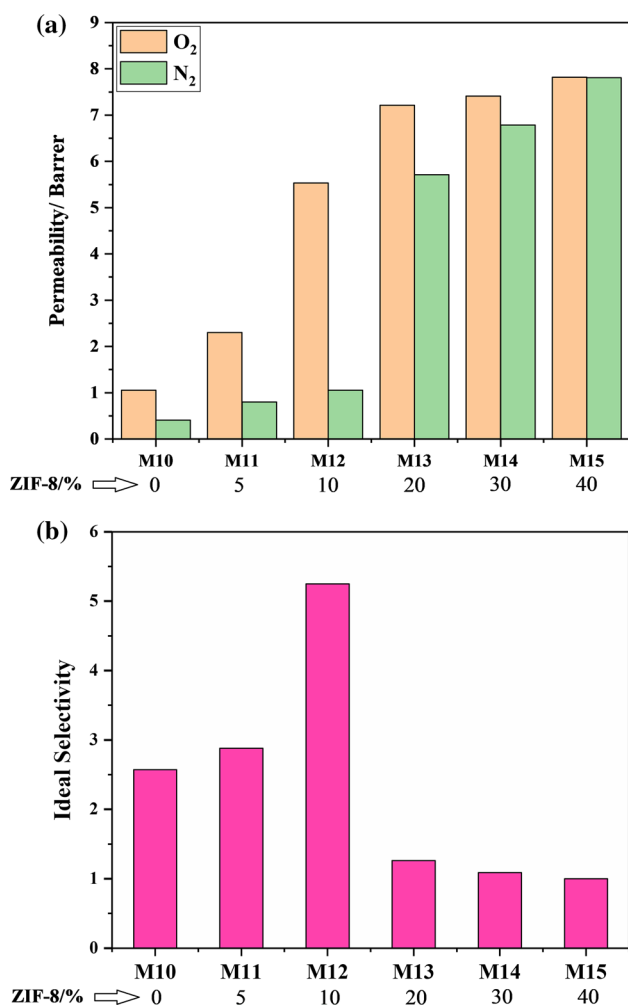


Fig. 15 a Permeability of O₂ and N₂ through mixed matrix hollow fiber membranes containing different ZIF-8 content (M10–M15), and b ideal selectivity of O₂/N₂ separation using M10–M15

illustrates the permeability of the prepared membranes including the bare PES membrane and MMMs containing different MOF content. As shown in this figure, the oxygen and nitrogen permeability have rising trends with the filler content, and the bare polymer showed the lowest permeability. Permeability increment with MOF filler content has been observed for different MOFs in the previous studies (Basu et al. 2011). From M10 (0%) to M12 (10%) the increment in the O₂ permeability is higher than that of N₂, which leads to increment in ideal selectivity. This could be due to smaller kinetic diameter of O₂ (0.346 nm) than N₂ which is comparable with pore aperture of ZIF-8 (0.34 nm) particles exposed to gas molecules in the inner and outer layer of fibers. It should be noted that the small difference in kinetic diameters of O₂ and N₂ (0.346 and 0.364 nm, respectively) shows that the separation of O₂/N₂ using only sieving mechanism is difficult. Therefore, aside from the sieving effect, the improved selectivity of M12 (10%) in comparison with the bare PES

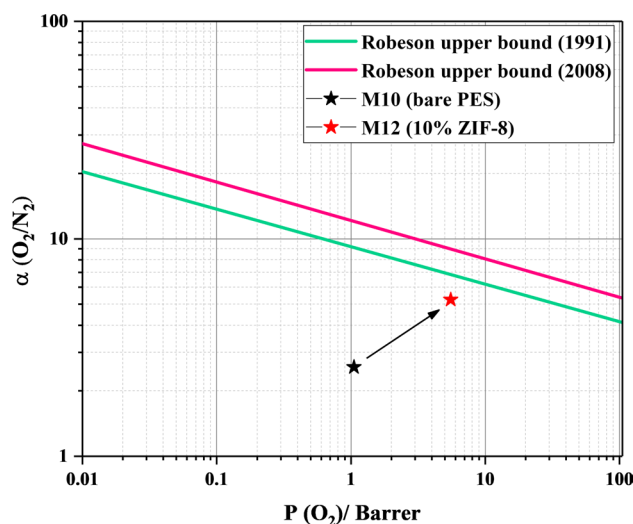


Fig. 16 O₂/N₂ selectivity versus O₂ permeability for M10 and M12 membranes along with Robeson upper bound

membrane could be attributed to the higher solubility selectivity as reported in the literature (Liu et al. 2019). But the permeability trend becomes reverse from M13 to M15, so that a sudden increase could be seen in N₂ permeability while the O₂ permeability rises with lower rate which leads to decreasing of selectivity from (M13 with 20% ZIF-8 to M15 with 40% ZIF-8). Therefore, the ideal selectivity becomes even lower than that of pure PES membrane. When the amount of filler in the polymer matrix is too large, the agglomeration of ZIF-8 particles occurs which leads to create defects in the MMMs. Fig. S12 shows the SEM image of agglomerated ZIF-8 particles and sieve-in-a-cage defect in M15 sample. These defects could explain the descending trend of selectivity with ZIF-8 content (higher than 10%).

The Robeson upper bound, and gas separation performance of the M10 (bare PES hollow fiber membrane) and M12 (with 10% ZIF-8 which had the best performance in this study) have been shown in Fig. 16. It shows that embedding of ZIF-8 particles at the optimum concentration could improve the MMM performance and the resultant operating point become closer to the Robeson upper bound.

Table 5 presents the comparison between the performance of MMM fabricated in this study and gas separation membranes (MMM or pure polymer membranes) reported in literature. As could be seen, both permeability and selectivity obtained in this work are almost in the range reported in the literature. The differences between the data could be attributed to the various parameters contribute in the gas separation performance of membranes such as polymer concentration, coating concentration and thickness, etc. It should be noted that hollow fiber configuration has some important benefits over flat sheet type for gas separation applications, in the same condition.

Table 5 Comparison of gas separation performance of bare polymer membranes and MMMs with different fillers

No	Membrane configuration	Symmetric/asymmetric	Polymer matrix	Filler	O ₂ permeability (Barrer)/Permeance (GPU)	O ₂ /N ₂ selectivity (ideal or mixed gas)	Ref
1	Flat sheet	Asymmetric	PSf	Pillared cloisite 15A	19.47 GPU	4.96	Natarajan et al. (2020)
2	Flat sheet	Dense	PSf	ZIF-8	6.1 Barrer	3.5	Burmann et al. (2014)
3	Flat sheet	Dense	PSf	MIL-101	> 6 Barrer	5–6	Jeazet et al. (2012)
4	Flat sheet	Asymmetric	PSf	ZIF-8	18.083 Barrer	2.95	Bagri and Mansourpanah (2021)
				NH ₂ -ZIF-8	9.98 Barrer	4.97	
				Thermal ZIF-8	13.42 Barrer	5.5	
5	Flat sheet	Dense	PSf	ZIF-8/silicalite-1	~ 1.75 Barrer	~ 7	Zornoza et al. (2011)
		Dense		HKUST-1/Silicalite-1	~ 1.7 Barrer	~ 8.0	
6	Hollow fiber	Asymmetric	PSf	Zeolite templated carbon	14 GPU	2.78	Wijiyanti et al. (2019)
7	Hollow fiber	Asymmetric	Matrimid/PSf (dual layer)	–	9.36 GPU	7.55	Ding et al. (2008)
8	Hollow fiber	Asymmetric	PES	–	20.33 GPU	3.13	Liu et al. (2017)
9	Hollow fiber	Asymmetric	PES	–	14.3 GPU	6.8	Wang et al. (2000)
10	Hollow fiber	Asymmetric	PES	–	15.7 GPU	5.8	Wang et al. (1996)
11	Hollow fiber	Asymmetric	PES	ZIF-8	5.53 Barrer	5.25	This Work

Conclusion

In this study, the effects of fabrication parameters on the morphology of hollow fiber membranes were examined. The selected parameters were polymer concentration, dope/bore flow rate ratios, and bore fluid composition during the spinning process. All these factors playing critical role determining the membrane characteristics (morphology, thickness and porosity), but results revealed that dope/bore fluid flow rate is the dominant factor determining the porosity of the membranes. At the fixed condition, mixed matrix membranes were fabricated at six level of ZIF-8 condition. These MMMs were used for O₂/N₂ separation through constant volume-variable pressure method. Results showed that the MMM with 10% of ZIF-8 has the best performance so that its perm-selectivity approaches to the Robeson upper bound.

Supplementary Information The online version contains supplementary material available at <https://doi.org/10.1007/s11696-021-01642-7>.

Funding Not applicable.

Declaration

Conflict of interest On behalf of all authors, the corresponding author states that there is no conflict of interest.

References

- Amooghini AE, Omidkhan M, Sanaeepour H, Kargari A (2016) Preparation and characterization of Ag⁺ ion-exchanged zeolite-Matrimid®5218 mixed matrix membrane for CO₂/CH₄ separation. *J Energy Chem* 25:450–462. <https://doi.org/10.1016/j.jechem.2016.02.004>
- Aroon M, Ismail A, Matsuura T, Montazer-Rahmati M (2010) Performance studies of mixed matrix membranes for gas separation: a review. *Sep Purif Technol* 75:229–242. <https://doi.org/10.1016/j.seppur.2010.08.023>
- Azam SU, Hussain A, Farrukh S, Noor T, Liu Y (2020) Enhancement in the selectivity of O₂/N₂ via ZIF-8/CA mixed-matrix membranes and the development of a thermodynamic model to predict the permeability of gases. *Environ Sci Pollut Res*. <https://doi.org/10.1007/s11356-020-08778-1>
- Bagri F, Mansourpanah Y (2021) Improvement of the performance of PDMS top layer of mixed matrix membrane incorporated with treated ZIF-8 for gas separation. *J Membr Sci Res* 7:111–117. <https://doi.org/10.22079/jmsr.2020.122067.1348>
- Bastani D, Esmaeili N, Asadollahi M (2013) Polymeric mixed matrix membranes containing zeolites as a filler for gas separation applications: a review. *J Ind Eng Chem* 19:375–393. <https://doi.org/10.1016/j.jiec.2012.09.019>
- Basu S, Cano-Odena A, Vankelecom I (2011) MOF-containing mixed-matrix membranes for CO₂/CH₄ and CO₂/N₂ binary gas mixture separations. *Sep Purif Technol* 81:31–40. <https://doi.org/10.1016/j.seppur.2011.06.037>
- Burmann P, Zornoza B, Téllez C, Coronas J (2014) Mixed matrix membranes comprising MOFs and porous silicate fillers

- prepared via spin coating for gas separation. *Chem Eng Sci* 107:66–75. <https://doi.org/10.1016/j.ces.2013.12.001>
- Chen X, Kaliaguine S, Rodrigue D (2019) Polymer hollow fiber membranes for gas separation: a comparison between three commercial resins. *AIP Conference Proceeding* 70003: 1–5. <https://doi.org/10.1063/1.5121669>
- Cui Z, Muralidhara H (2010) *Membrane technology: A practical guide to membrane technology and applications in food and bioprocessing*. Butterworth-Heinemann, Oxford
- Dai Y, Johnson J, Karvan O, Sholl D, Koros W (2012) Ultem®/ZIF-8 mixed matrix hollow fiber membranes for CO₂/N₂ separations. *J Membr Sci* 401–402:76–82. <https://doi.org/10.1016/j.memsci.2012.01.044>
- Ding X, Cao Y, Zhao H, Wang L, Yuan Q (2008) Fabrication of high performance matrimid/polysulfone dual-layer hollow fiber membranes for O₂/N₂ separation. *J Membr Sci* 323:352–361. <https://doi.org/10.1016/j.memsci.2008.06.042>
- Ebrahimi S, Mollaiy-Berneti S, Asadi H, Peydayesh M, Akhlaghian F, Mohammadi T (2016) PVA/PES-amine-functional graphene oxide mixed matrix membranes for CO₂/CH₄ separation: experimental and modeling. *Chem Eng Res Des* 109:647–656. <https://doi.org/10.1016/j.cherd.2016.03.009>
- Eruar I, Keskin S (2011) Screening metal organic framework-based mixed-matrix membranes for CO₂/CH₄ separations. *Ind Eng Chem Res* 50:12606–12616. <https://doi.org/10.1021/ie201885s>
- Feijani EA, Mahdavi H, Tavasoli A (2015) Poly(vinylidene fluoride) based mixed matrix membranes comprising metal organic frameworks for gas separation applications. *Chem Eng Res Des* 96:87–102. <https://doi.org/10.1016/j.cherd.2015.02.009>
- Hadi A, Karimi-sabet J, Dastbaz A (2020) Parametric study on mixed solvent synthesis of ZIF-8 nano- and micro-particles for CO adsorption: a response surface study. *Front Chem Sci Eng* 14:579–594. <https://doi.org/10.1007/s11705-018-1770-3>
- Han J, Lee W, Choi JM, Patel R, Min BR (2010) Characterization of polyethersulfone/polyimide blend membranes prepared by a dry/wet phase inversion: precipitation kinetics, morphology and gas separation. *J Membr Sci* 351:141–148. <https://doi.org/10.1016/j.memsci.2010.01.038>
- Hasanajili S, Latifzadeh M, Bahmani M (2017) Permeation properties of CO₂ and CH₄ in asymmetric polyethersulfone/polyesterurethane and polyethersulfone/polyetherurethane blend membranes. *Chin J Chem Eng* 25:1750–1759. <https://doi.org/10.1016/j.cjche.2017.07.011>
- Jeazet HBT, Staudt C, Janiak C (2012) A method for increasing permeability in O₂/N₂ separation with mixed-matrix membranes made of water-stable MIL-101 and polysulfone. *Chem Commun* 48:2140–2142. <https://doi.org/10.1039/C2CC16628C>
- Junaidi M, Leo C, Ahmad A, Kamal S, Chew T (2014) Carbon dioxide separation using asymmetric polysulfone mixed matrix membranes incorporated with SAPO-34 zeolite. *Fuel Process Technol* 118:125–132. <https://doi.org/10.1016/j.fuproc.2013.08.009>
- Li Q, Wang J, Liu W, Zhuang X, Liu J, Fan G, Li B, Lin W, Man J (2015) A new (4,8)-connected topological MOF as potential drug delivery. *Inorg Chem Commun* 55:8–10. <https://doi.org/10.1016/j.inoche.2015.02.023>
- Liu X, Liu H, Li P (2017) Effect of polymer dope concentration on the morphology and performance of PES/PDMS hollow fiber composite membrane for gas separation. *J Mater Sci* 1:555573. <https://doi.org/10.19080/JOJMS.2017.01.555573>
- Liu Y, Zhang J, Tan X (2019) High performance of PIM-1/ZIF-8 composite membranes for O₂/N₂ separation. *ACS Omega* 4:16572–16577. <https://doi.org/10.1021/acsomega.9b02363>
- Natarajan P, Sasikumar B, Elakkiya S, Arthanareeswaran G, Ismail AF, Youravong W, Yuliwati E (2020) Pillared cloisite 15A as an enhancement filler in polysulfone mixed matrix membranes for CO₂/N₂ and O₂/N₂ gas separation. *J Nat Gas Sci Eng* 86:103720. <https://doi.org/10.1016/j.jngse.2020.103720>
- Nath K (2008) *Membrane separation processes*. PHI Learning Pvt. Ltd., Delhi
- Nunes S, Peinemann K (2006) *Membrane technology in the chemical industry*. Wiley, Weinheim, Germany
- Pabby A, Rizvi S, Reuena A (2008) *Handbook of membrane separations: chemical, pharmaceutical, food, and biotechnological applications*. CRC Press Boca Raton
- Park C, Tocci E, Fontananova E, Bahattab M, Aljlil S, Drioli E (2016) Mixed matrix membranes containing functionalized multiwalled carbon nanotubes: Mesoscale simulation and experimental approach for optimizing dispersion. *J Membr Sci* 514:195–209. <https://doi.org/10.1016/j.memsci.2016.04.011>
- Shahid S, Nijmeijer K, Nehache S, Vankelecom I, Deratani A, Quemenner D (2015) MOF-mixed matrix membranes: precise dispersion of MOF particles with better compatibility via a particle fusion approach for enhanced gas separation properties. *J Membr Sci* 492:21–31. <https://doi.org/10.1016/j.memsci.2015.05.015>
- Simone S, Figoli A, Criscuoli A, Carnevale M, Alfadul S, Al-Romaih H, Shabouna FA, Al-Harbi O, Drioli E (2014) Effect of selected spinning parameters on PVDF hollow fiber morphology for potential application in desalination by VMD. *Desalination* 344:28–35. <https://doi.org/10.1016/j.desal.2014.03.004>
- Wang D, Li K, Teo WK (1996) Polyethersulfone hollow fiber gas separation membranes prepared from NMP/alcohol solvent systems. *J Membr Sci* 115:85–108. [https://doi.org/10.1016/0376-7388\(95\)00312-6](https://doi.org/10.1016/0376-7388(95)00312-6)
- Wang D, Li K, Teo WK (2000) Highly permeable polyethersulfone hollow fiber gas separation membranes prepared using water as non-solvent additive. *J Membr Sci* 176:147–158. [https://doi.org/10.1016/S0376-7388\(00\)00419-1](https://doi.org/10.1016/S0376-7388(00)00419-1)
- Wijiyanti R, Ubaidillah AN, Gunawan T, Karim ZA, Ismail AF, Smart S, Lin R, Widiastuti N (2019) Polysulfone mixed matrix hollow fiber membranes using zeolite templated carbon as a performance enhancement filler for gas separation. *Chem Eng Res Des* 150:274–288. <https://doi.org/10.1016/j.cherd.2019.08.004>
- Zhang C, Zhang K, Xu L, Labreche Y, Kraftschik B, Koros W (2014) Highly scalable ZIF-based mixed-matrix hollow fiber membranes for advanced hydrocarbon separations. *AIChE J* 60:2625–2635. <https://doi.org/10.1002/aic.14496>
- Zhao C, Xue J, Ran F, Sun S (2013) Modification of polyethersulfone membranes—a review of methods. *Prog Mater Sci* 58:76–150. <https://doi.org/10.1016/j.pmatsci.2012.07.002>
- Zornoza B, Seoane B, Zamaro JM, Téllez C, Coronas J (2011) Combination of MOFs and zeolites for mixed-matrix membranes. *ChemPhysChem* 12:2781–2785. <https://doi.org/10.1002/cphc.201100583>

Publisher's Note Springer Nature remains neutral with regard to jurisdictional claims in published maps and institutional affiliations.